# Influence of point defects on the electronic properties of boron nitride nanosheets

**ARTICLE** *in* JOURNAL OF MOLECULAR MODELING · SEPTEMBER 2011

Impact Factor: 1.74 · DOI: 10.1007/s00894-011-1233-y · Source: PubMed



**4 AUTHORS**, INCLUDING:

Ernesto Chigo
Meritorious Autonomous University of Puebla
**71** PUBLICATIONS **360** CITATIONS
SEE PROFILE

Alejandro Escobedo Morales
Meritorious Autonomous University of Puebla
**22** PUBLICATIONS **320** CITATIONS
SEE PROFILE

Gregorio H. Cocoletzi
Meritorious Autonomous University of Puebla
**121** PUBLICATIONS **510** CITATIONS
SEE PROFILE

J Mol Model (2012) 18:2175–2184
DOI 10.1007/s00894-011-1233-y

ORIGINAL PAPER

# Influence of point defects on the electronic properties of boron nitride nanosheets

**Ernesto Chigo Anota · Ramses E. Ramírez Gutiérrez · Alejandro Escobedo Morales · Gregorio Hernández Cocoletzi**

Received: 4 June 2011 / Accepted: 24 August 2011 / Published online: 27 September 2011


**Abstract** Density functional theory was utilized to study the electronic properties of boron nitride (BN) sheets, taking into account the presence of defects. The structure considered consisted of a central hexagon surrounded by alternating pentagons (three) and heptagons (three). The isocoronene cluster model with an armchair edge was used with three different chemical compositions. In the first structure, three B–B bonds were formed where one B in the dimer was part of the central hexagon. In the second structure, three N–N–N bonds were formed at the periphery of the cluster, around the central hexagon. In the third structure, three N–N bonds were formed in a similar fashion to the first model. Our results indicated that the third structure was the most stable configuration; this exhibited planar geometry, semiconductor behavior, and ionic character. To explore the effects of doping, we replaced B and N atoms with C atoms, considering different atomic positions in the central hexagon. When an N atom was replaced with a C atom, the new structure was a semiconductor, but when a B atom was replaced with a C atom, the new structure was a semimetal. At the same time, the polarity increased, inducing covalent behavior. Replacing two N atoms with two C atoms also resulted in a semiconductor, while replacing two B atoms with two C atoms yielded a semimetal; in both cases the bonding was covalent. When three B (three N) atoms of the central hexagon were replaced with three C atoms, the new structure exhibited a transition to a conductor (remained a semiconductor) with low polarity. When monovacancies (N) and divacancies (B and N) were inserted into the lattice, the system was transformed into a covalent semiconductor. Finally, the electrostatic potential surface was calculated in order to explore intermolecular properties such as the charge distribution, which showed how the reactivity of the boron nitride sheets was affected by doping and orbital hybridization.

**Keywords** Boron nitride · DFT theory · Isocoronene · Electrostatic potential

E. C. Anota (✉) · A. E. Morales
Facultad de Ingeniería Química, Cuerpo Académico de Ingeniería en Materiales, Benemérita Universidad Autónoma de Puebla, Ciudad Universitaria, San Manuel, Puebla, Código Postal 72570, México
e-mail: echigoa@yahoo.es

R. E. R. Gutiérrez
Facultad de Ciencias Químicas, Benemérita Universidad Autónoma de Puebla, CP72570 Puebla, Pue, México

G. H. Cocoletzi
Instituto de Física 'Luís Rivera Terrazas', Benemérita Universidad Autónoma de Puebla, Apartado Postal J-48, Puebla 72570, México

## Introduction

Graphene and graphene-like 2D layers have attracted the attention of scientists due to their suitability for applications in the technology industry. Boron nitride hexagonal (h-BN) sheets were prepared experimentally for the first time in 2005 by Geim and collaborators [1]. Since then, this material has led to the possibility of fabricating new optoelectronic devices, as recently reported [2]. Even though this material has been the subject of many investigations, there are still no reports of any inves-

tigations of lattice defects in h-BN sheets, performed in a similar fashion to those done for graphene sheets [3]. In a recent paper, Akcöltekin [4] performed theoretical and experimental investigations of lattice defects of graphene. These studies of defect engineering were performed using ion irradiation (Fig. 1) [5], and the isocoronene cluster model [6] ($C_{24}H_{12}$, Fig. 2a) was used to represent the d-BN armchair edge [7].

In a recent paper, Chigo [8] used the armchair edge circular model to investigate 2D carbon atomic structures, taking into account the presence of N atoms as doping atoms. Similar atomic configurations have been used to study the atomic structures of GaAlN and GaInN alloys [9], III-A nitrides [10], the adsorption of $H_2O$ onto 2D h-BN [11], the doping of h-BN sheets with Li and F [12], the adsorption of $O_3$ onto h-BN sheets [13], the atomic structure of silicon carbide (either pure or with defects) [14], the effects of chemically modifying boron nitride oxide sheets, and vacancies and nitrogen dopants in boron nitride oxide.

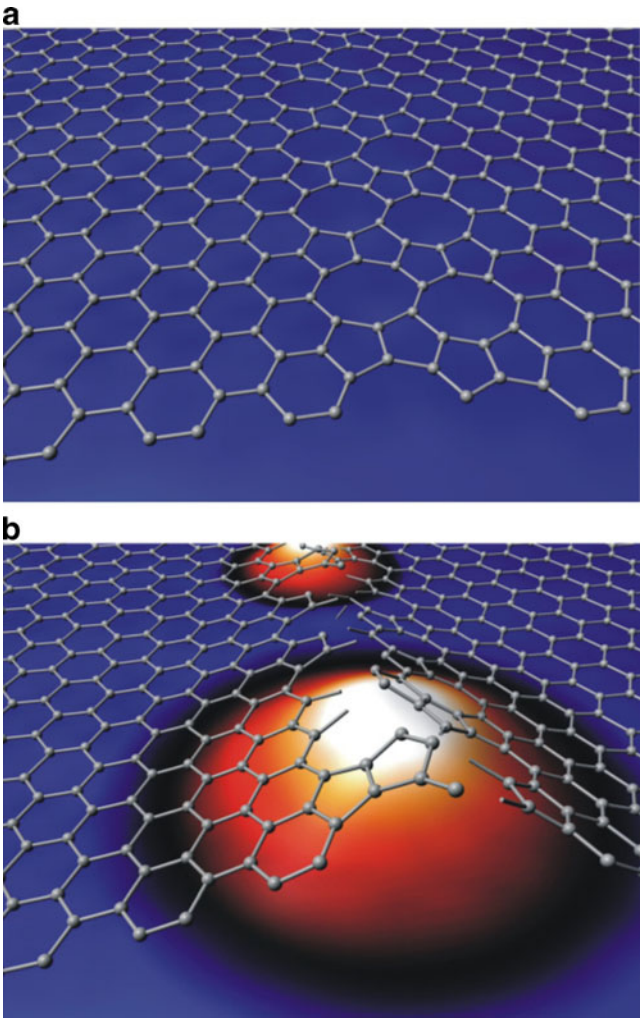


**Fig. 1** Lattice model used to represent lattice defects in graphene. The graphene structure can be fabricated by ion irradiation [4]

Motivated by the work in [4], we investigated the atomic structure of h-BN sheets, taking into account lattice defects. The results of this investigation are summarized in this paper. We considered the atomic structure of the sheets to consist of a central hexagon surrounded by alternating pentagons (three) and heptagons (three) with three different chemical compositions, as depicted in Fig. 2b–d. Configuration 1 had three B–B bonds; configuration 2 had three N–N–N bonds at the periphery, around the central hexagon; while configuration 3 had three N–N bonds arranged in a similar fashion to configuration 1. We also explored the electronic properties of BN sheets as a function of the doping. To do this, we replaced one to three of the B or N atoms of the central hexagon with carbon (C) atoms. In addition, the effects of mono- and divacancies on the stable structures were studied. Finally, the chemical reactivities of the h-BN sheets were analyzed in terms of their electrostatic potential surfaces.

## Computational methods

We performed first-principles total energy calculations to study boron nitride sheets, accounting for vacancies and doping effects, according to a procedure presented elsewhere [8–14]. Our calculations were performed using density functional theory (DFT) [15–19], as implemented in the DMOL$^3$ code [20]. The exchange and correlation energies were treated according to the local density approximation (LDA) with Perdew–Wang (PWC) [21] parametrization in the all-electron formalism, assuming that spin effects were unimportant for our system.

In the calculations, we used a double numeric polarized (DNP) atomic base (this includes a *p* orbital of hydrogen and *d* orbitals of carbon, boron, and nitrogen) for the core [20, 22, 23], with multiplicity equal to 1 (singlet) and zero charge (neutral) for the $B_{12}N_{12}H_{12}$ cluster, which has a base of 0.946 nm and a height of 0.98 nm (Fig. 2), in the absence of any doping. In the next step, a doped structure with a charge equal to zero and a multiplicity equal to 2 was considered, and the same conditions were applied to investigate structures with mono- and divacancies. Similar to the hexagonal boron nitride (h-BN) sheets, we apply the local density approximation to these d-BN sheets, assuming that spin does not affect their atomic and electronic structure.

The cutoff orbital radius used in the calculations was 0.40 nm, the self-consistency tolerance was $1.0\times10^{-6}$ Ha, and the relaxation procedure took the positive vibration frequency criterion into account [24]. We

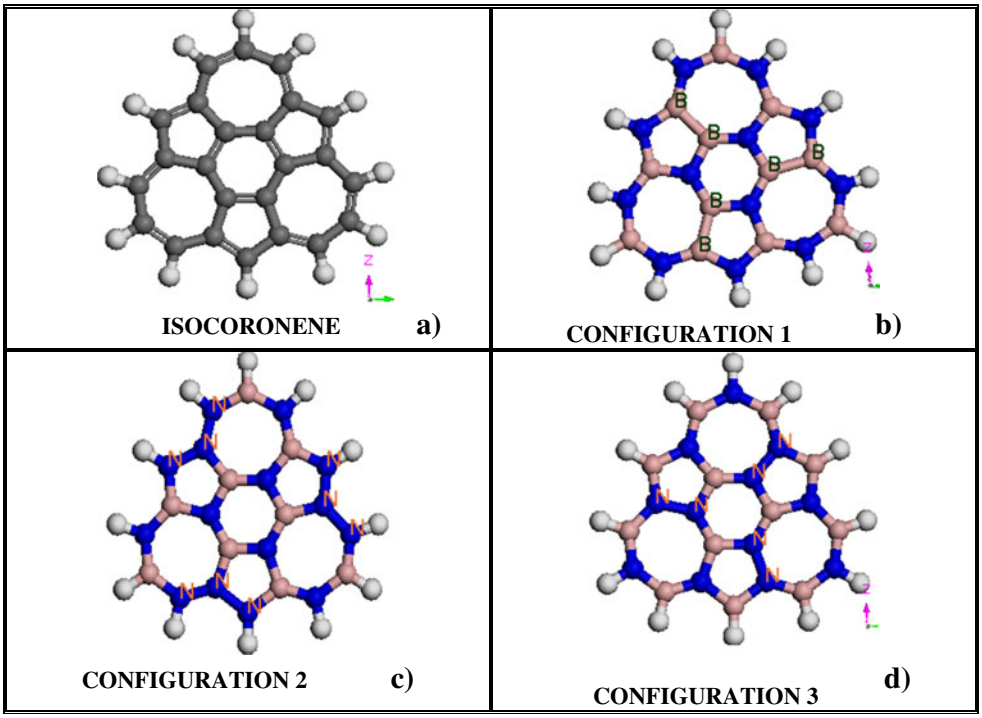


**Fig. 2** **a** Coronene isomer ($C_{24}H_{12}$) model that was used to represent graphene. **b–d** Initial atomic geometries of the boron nitride nanosheets

determined the most stable configurations, polarities (dipole moments), binding energies, and energy gaps. Energy gaps were calculated as the energy difference between the HOMO and LUMO orbital energies. To validate our structural model, we used a procedure described in [25] for determining the cohesive energy for the following models: naphthalene, pyrene, coronene, and the cluster $B_{27}N_{27}H_{18}$. The value of the cohesive energy was 1.66 a.u./atom [26], assuming that size does not affect electronic properties.

To elucidate the static charge distribution, we calculated the electrostatic potential at van der Waals distances [27]. It is well known that any distribution of electrical charge, such as those of electrons or nuclei of molecules, creates an electrical potential in the surrounding space. This may be considered the potential of the molecule, which interacts with a point electrical charge [28]. A variety of methods to calculate the electrostatic potential are currently available in the literature, which display different levels of accuracy. In the present work, the molecules were investigated with the hybrid functional B3LYP [29] and the 6-31+G(d,p) [30, 31] basis using the GAUSSIAN03 [32] program. In the calculations, the electrostatic potential surfaces of the rings were generated by mapping the electrostatic potentials onto isosurfaces of the molecular electron density between 0.02 and 0.04 a.u. and by color coding using the program gOpenMol [33] to visualize the molecules.

## Results and discussion

The isocoronene model of boron nitride sheets suggested the possibility of generating lattice defects in the structure with the formation of pentagons, hexagons, and heptagons.

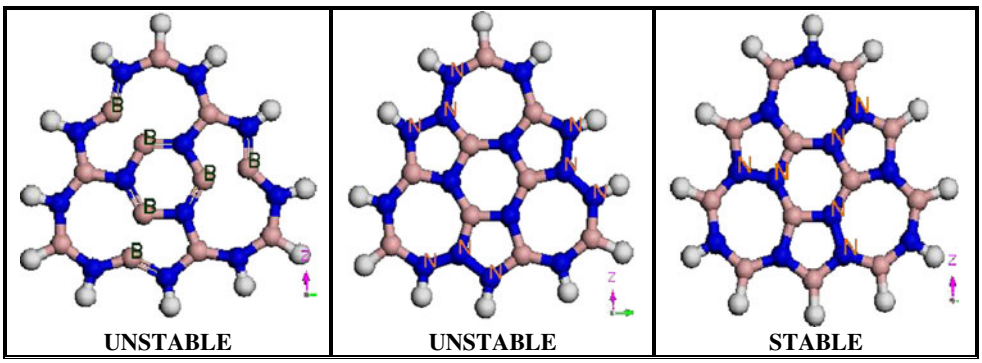


**Fig. 3** The relaxed atomic geometries of boron nitride nanosheets

To carry out calculations, we applied the isocoronene cluster model with the armchair edge to three different chemical compositions. In the first model, three B–B bonds were formed, where the B atom of the dimer was part of the central hexagon. In the second model, three N–N–N bonds were formed at the periphery, around the central hexagon. The third model was similar to the first structure, but three N–N bonds were formed instead.

Studies of vacancy effects indicated that model 3 was the model with the lowest minimum energy (see Fig. 3), so this was considered the ground state of the system. In this stable configuration, the B–N bonds showed *sp* hybridization, which is very similar to what is reported in the literature [8, 13]. The system had no overall charge and the multiplicity was 1 (within the LDA formalism, with restricted spin). The structure exhibited a regular geometry, in contrast to the irregular geometry of graphene (as represented by isocoronene) at the C–C bond; see Table 1.

Doping effects were investigated, as shown in Fig. 4a and b. We replaced 4.16% of the B (N) by C, which led to stable, planar, 2D structures. The *sp* orbital hybridization of the C–N bonds alternated between *sp* and $sp^2$ throughout the entire lattice (Fig. 4a). Similarly, *sp* hybridization of the B–C bonds alternates with the $sp^2$ hybridization of the C–N bonds (Fig. 4b). These results agree with those obtained for CN structures with circular, rectangular, and triangular [34] shapes.

Replacing two B or N atoms with two C atoms also resulted in stable geometries, with $sp^2$ hybridization observed for the N–C bonds and *sp* hybridization for the B–C bonds; see Fig.4c.

Additional studies of the effects of doping were performed. We explored the structure obtained by replacing 25% of the central hexagon's atoms with C atoms, thus producing the following chemical composition: $B_9C_6N_9H_{12}$. This system had the geometry of model 3 (see Fig. 4c). After structural relaxation, the B–N bond length was 1.39 Å (in the central hexagon), which is somewhat different from the value of 1.44 Å obtained for the B–N bonds in the pentagons and 1.43 Å for those in the heptagons. These values are similar to those observed for hexagonal BN sheets with no defects [8]. The B–N bonds display *sp* hybridization and the C–C bonds show $sp^2$ hybridization.

When two B (N) atoms in the central hexagon are substituted by two C atoms, the structure behaves as semiconductor (semimetal) with an energy gap of 0.82 eV (0.45 eV) and a high polarity of $991.8\times10^{-3}$ ($1167.2\times10^{-3}$) D.

Doping with three C atoms is represented in Fig. 4d. Again, we replaced B and N atoms independently. After relaxation, in the stable atomic configurations, two of the three N–C bonds displayed $sp^2$ hybridization, while and the B–C bonds exhibited *sp* hybridization.

Monovacancies resulting from the absence of a B (N) atom induced $sp^2$ hybridization in B–N bonds inside pentagons, hexagons, and heptagons (Fig. 4f). However, divacancies (see Fig. 4e) led to a stable lattice structure with two hexagons, one pentagon, one tetragon, and one octagon, which presented bonding based on *sp* hybridization. This is similar to what was observed in a graphene oxide layer.

We determined the energy gap (3.42 eV) of the BN sheet with no defects based on the energy difference between the HOMO and LUMO orbitals. This energy gap indicates that the structure behaves as a semiconductor with ionic character, and has a dipole moment of $4.3\times10^{-3}$ D. This result is in accord with the experimental value for the hexagonal BN sheet in the presence of vacancies [35]. In contrast, replacing the B site of the central hexagon with a C atom yielded a covalent atomic geometry of high polarity ($1060.9\times10^{-3}$ D), similar to what has been reported for the BN oxide sheet [36]. When the N atom was replaced instead, the structure transformed from a semimetal (energy gap of 0.33 eV) into a semiconductor (energy gap of 1.97 eV).

Replacing the three B (N) atoms of the central hexagon with three C atoms produced a stable conductor (semiconductor) with ionic character.

The electrostatic potential $V(r)$ of a molecule, based on the static charge distributions of the nuclei and electrons within it, can be analyzed to predict the reactivity of the molecule [37]. If a molecule has an electron density $\rho(r)$, then its electrostatic potential at any point $r$ is given by

$$V(r) = \sum_{\mathrm{A}} \frac{Z_{\mathrm{A}}}{|R_{\mathrm{A}} - r|} - \int \frac{\rho(r')dr'}{|r' - r|} \quad (1)$$

Here, $Z_{\mathrm{A}}$ is the charge of nucleus A, located at $r = R_{\mathrm{A}}$. This potential has proven to be a particularly useful indicator of the sites or regions of a molecule to which an approaching electrophile will be attracted. It has been applied successfully to study interactions between reactants and to recognition in biological systems (e.g., in enzyme–substrate systems) [27, 37–39].

Using the approach described above, we characterized the electrostatic potential surface of the boron nitride sheet in terms of site-specific and global quantities. The calculated electrostatic potential surfaces for different BN models are presented in Figs. 5, 6, and 7. The electrostatic potential surface for model C1 is displayed in Fig. 5, where the positive (the red color represents boron atoms with an isosurface of 0.04 a.u.) and negative (the blue color represents nitrogen atoms with an isosurface of −0.02 a.u.) charge densities are clearly separated, indicating that there is no resonance effect. However, for model C2, as shown in Fig. 5c, it is possible to find $sp^2$ hybridization for the N–N–N bonds with high electron density (these are represented by

**Table 1** Optimized atomic geometries, dipolar moments, energy gaps, and binding energies of the nanosheets

| System | Bond distance (Å) | | | | | Dipolar moment ($\times 10^{-3}$ D) | Gap (HOMO–LUMO, eV) | Binding energy (eV) |
|---|---|---|---|---|---|---|---|---|
| | C–C | B–N | N–N | C–N | B–C | | | |
| [A]Isocoronene (graphene) | 1.41( hexagon)<br>1.39 (heptagon)<br>1.44 (pentagon) | | | | | 1.33 | 0.98 | 8.73 |
| $C_{54}H_{18}$ (graphene) | 1.41 | | | | | 2.9 | 1.94 | 19.18 |
| $C_{24}H_{12}$ [5] (graphene) | 1.41 | | | | | 0.2 | 4.06 | |
| $B_{12}N_{12}H_{12}$ [8] | | 1.44 | | | | 3.7 | 6.96 | 7.95 |
| $B_{27}N_{27}H_{18}$ (doping with hexagon C) | | 1.44 | | | | 13.4 | 4.84 | 17.16 |
| BNO C1 [33] | | 1.43<br>1.47 | | | | 1584 | 1.2 | 18.76 |
| BNO C2 [33] | | 1.44<br>1.45 | | | | 7200 | 2.4 | 18.88 |
| BN configuration 1 | | 1.43 | | | | 7.3 | 3.76 | Unstable structure |
| BN configuration 2 | | 1.43 | 1.38<br>1.41 | | | 8.0 | 3.16 | Unstable structure |
| BN<br>Configuration 3 | | 1.43 | | | | 4.3 | 3.42 | 7.64 |
| BN monovacancy | | | | | | | | |
| B | | 1.43 | 1.38 | | | 2159.5 | 0.23 | Unstable |
| N | | 1.43 | 1.38 | | | 1188.2 | 1.96 | 7.25 |
| BN divacancy (B,N) | | 1.43 | 1.43 | | | 118.6 | 3.59 | 6.99 |
| BN doped with C (replacing B) | | 1.43 | 1.41 | 1.36 | | 1060.9 | 0.33 | 7.55 |
| BN doped with C (replacing N) | | 1.43<br>1.45<br>1.47 | 1.41 | 1.37 | | 349.5 | 1.97 | 7.66 |
| BN hexagon doped with C | 1.39 | 1.43 | 1.40 | | | 2.4 | 2.87 | 7.93 |
| BN doped with 3C (replacing 3B) | | 1.44<br>1.45 | | | 1.49 | 2.2 | 0.0 | 7.73 |
| BN doped with 3C (replacing 3N) | | 1.44 | 1.39 | 1.37 | | 7.6 | 1.12 | 7.73 |
| BN doped with 2C (replacing 2B) | | 1.42 | 1.39 | 1.39 | | 1167.2 | 0.45 | 7.47 |
| BN doped with 2C (replacing 2B) | | 1.43 | 1.40 | 1.38 | 1.50 | 991.8 | 0.82 | 7.697 |

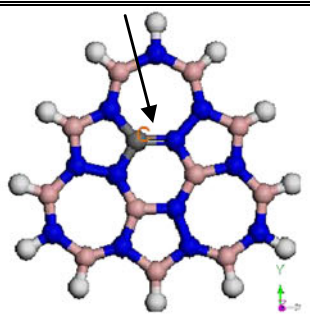

STABLE a)

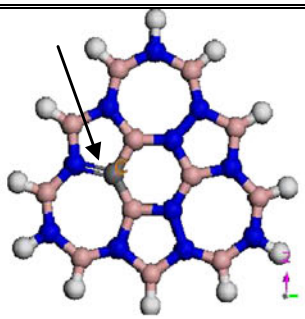

STABLE b)

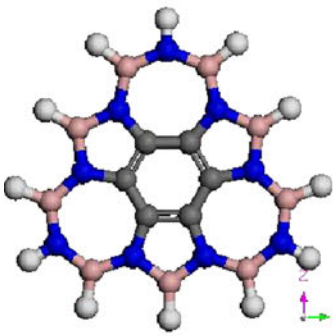

STABLE c)

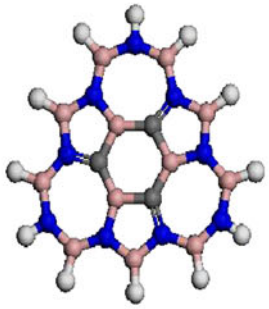

STABLE

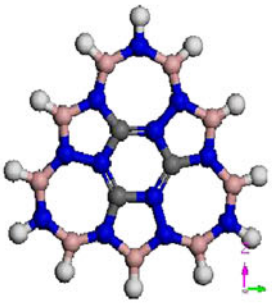

STABLE

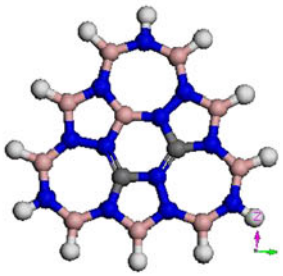

STABLE

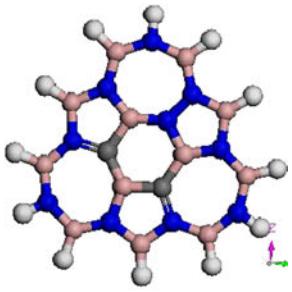

STABLE d)

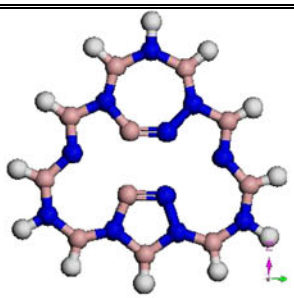

INITIAL

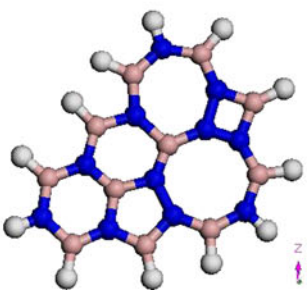

STABLE, FINAL e)

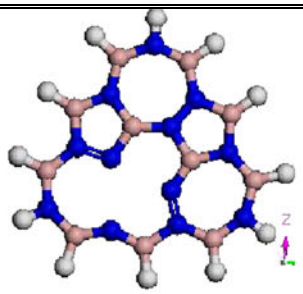

MONOVACANCY OF B
UNSTABLE (INITIAL AND FINAL)

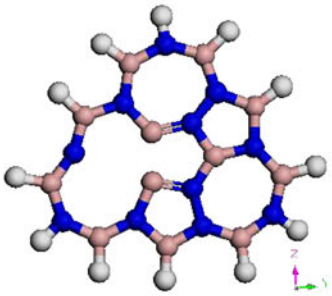

MONOVACANCY OF N
STABLE (INITIAL AND FINAL) f)

◀ **Fig. 4a–f** Atomic geometries of the boron nitride sheets after relaxation, taking into account carbon atom doping. Structures of the stable configurations are shown. **a** A carbon atom replaces a boron atom, **b** a carbon atom replaces a nitrogen atom, **c** doping of the central hexagon with carbon atoms, **d** replacing two or three B and N atoms with the equivalent number of C atoms, **e** initial and final geometries obtained with B and N divacancies, and **f** initial and final geometries of nanosheets with B and N monovacancies, respectively

the blue color, with an isosurface of −0.02 a.u.). Model C3 also displays $sp^2$ binding at the N–N bonds with the boron appearing as an isolated atom; similar effects are seen in carbon and boron/nitrogen [40, 41].

Similarly, we characterized the electrostatic potential surfaces of the different d-BN sheet models, as presented in Fig. 6. In the first model (see Fig. 6a), the atoms in the central ring have been replaced with carbon atoms, inducing distinctive charge distributions between the carbon atoms and between the carbons and the adjacent nitrogen atoms. The charge distribution due to the π electrons that move around the central benzene molecule is represented in a green color.

The model 1N by 1C (as presented in Fig. 6c), where one N atom in the central ring has been replaced with a carbon atom, shows similar electronegativities and hybrid-

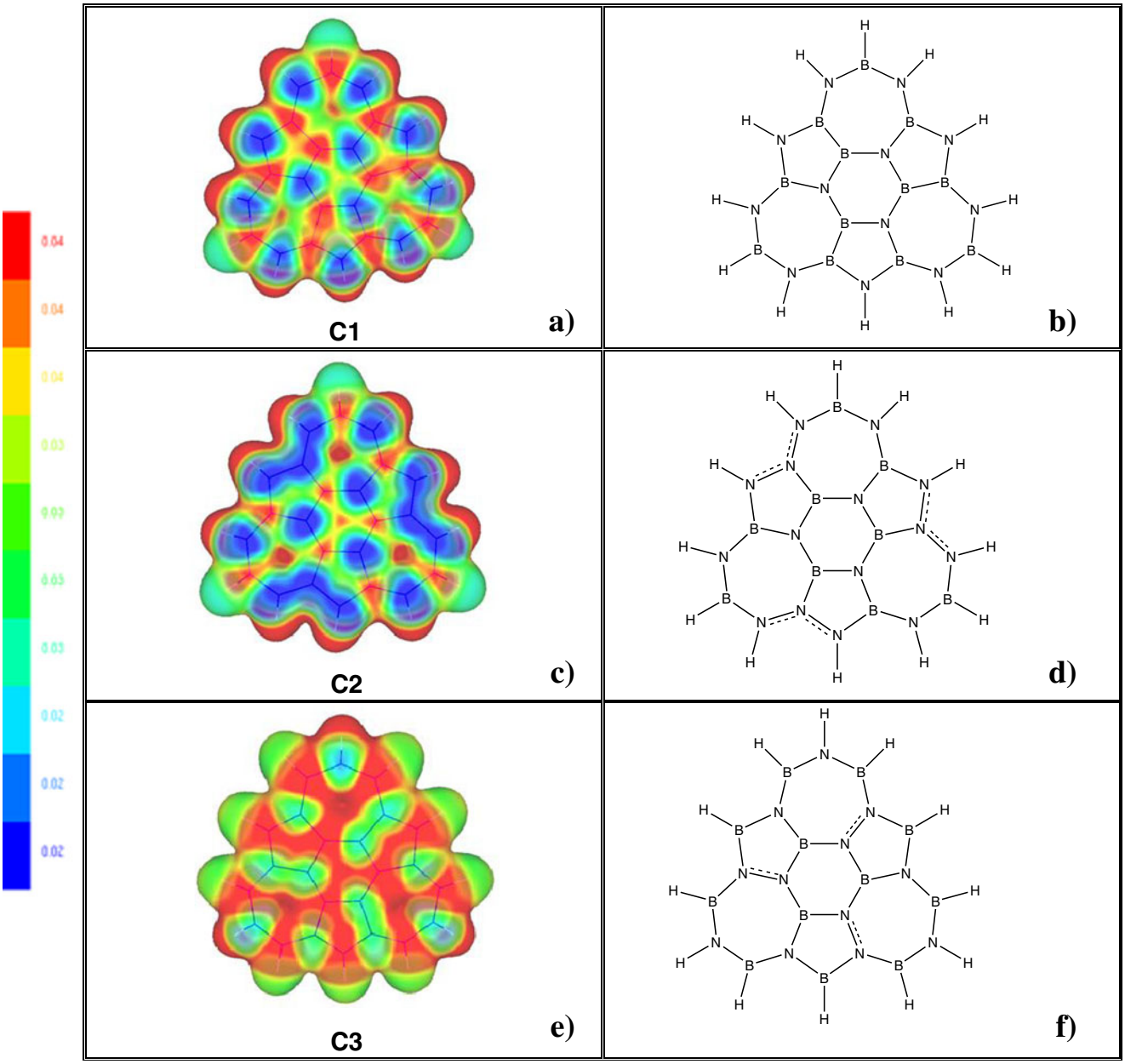


**Fig. 5a–f** Electrostatic potential surfaces for the three models C1, C2, and C3 (**a**, **c**, and **e**, respectively) used in the calculations. These represent boron nitride sheets with lattice defects. **b**, **d**, and **f** show the structural formulae of the models

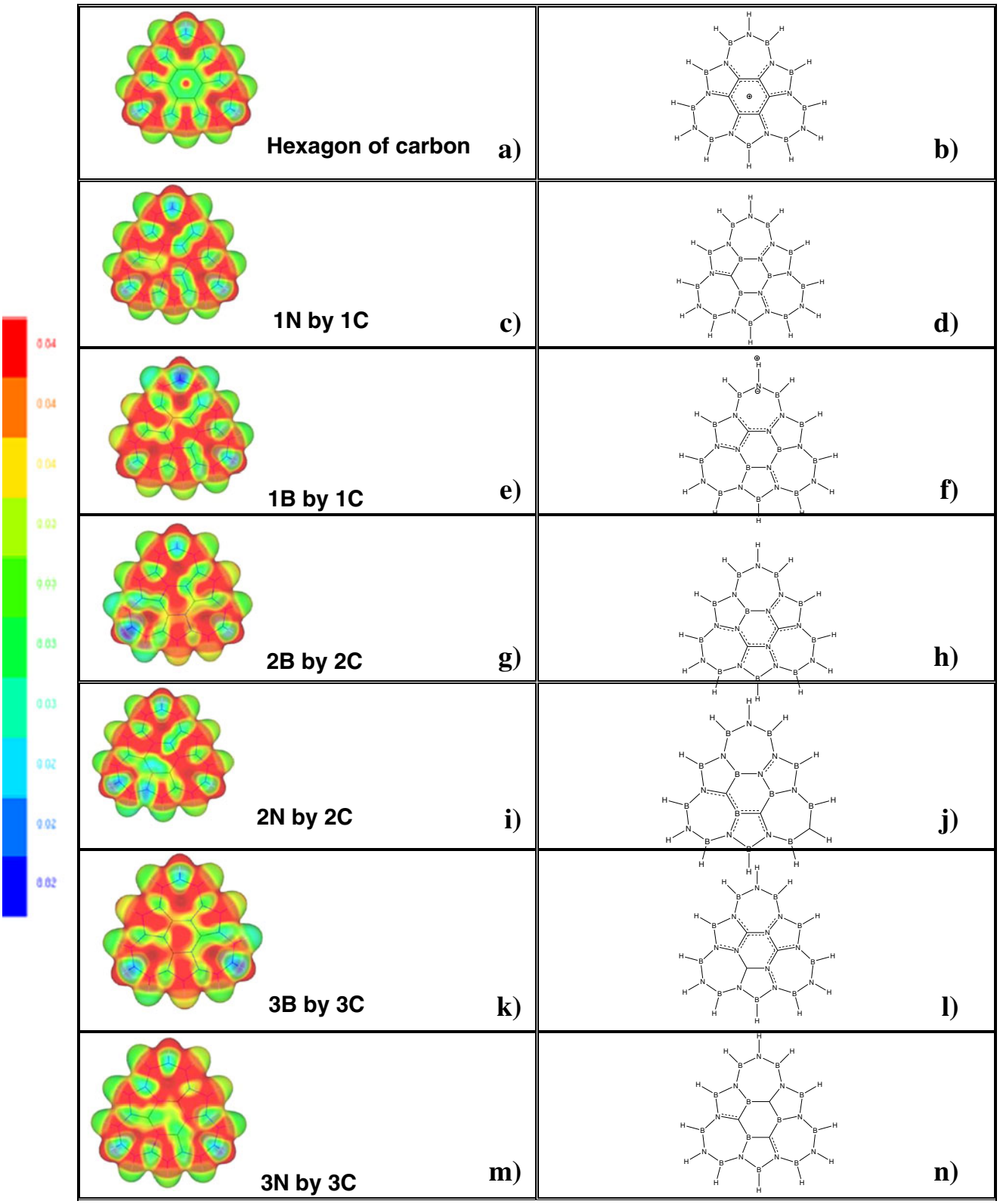


**Fig. 6a–n** Electrostatic potential surfaces of d-BN sheets that include doping. Each diagram represents a relaxed d-BN sheet that is doped with carbon atoms at a particular concentration (**a**, **c**, **e**, **g**, **i**, **k**, and **m**) and its corresponding structural formulae (**b**, **d**, **f**, **h**, **j**, **l**, and **n**)

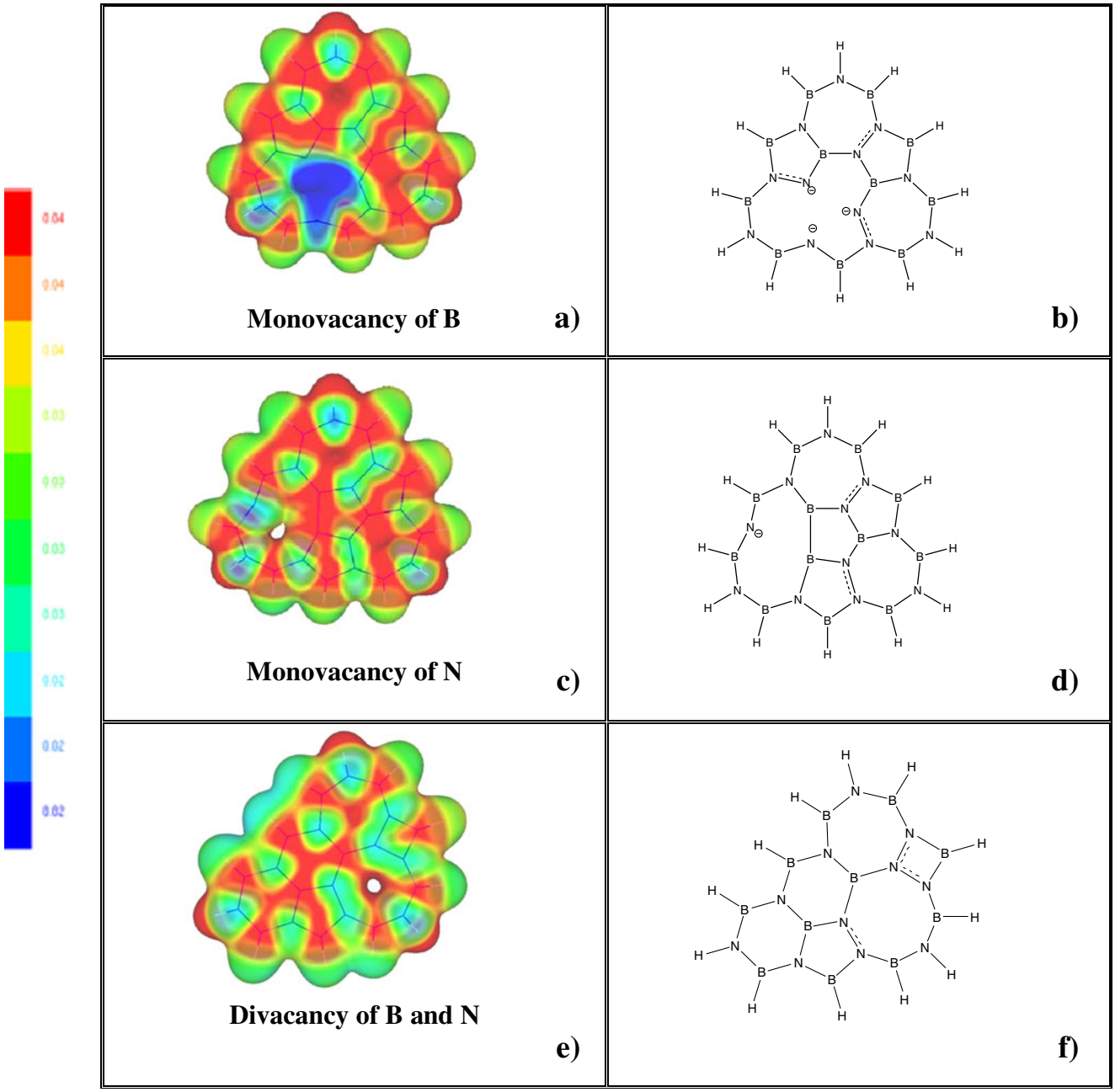


**Fig. 7a–f** Electrostatic potential surfaces of d-BN sheets with B (**a**) and N (**b**) monovacancies and with (B, N) divacancies (**c**) after atomic coordinate optimization, as well the corresponding structural formulae (**b**, **d**, and **f**, respectively)

izations to model C3. The hybridizations of the carbon and nitrogen atoms mean that C substitution barely changes the electrostatic potential surface of the sheet. The same behavior is observed when one B atom in the central ring is replaced with a C atom; the conjugation expands to include the nitrogen atoms adjacent to carbon, as depicted by the isosurface of 0.03 a.u. (shown as a green color in Fig. 6e).

Figure 6g represents the 2B by 2C model, and shows the charge distribution between the nitrogen and carbon atoms, and how the boron atoms are left isolated with positive charges. In contrast, in Fig. 6i, the charge distribution surrounding the boron atoms is a consequence of the environment. In the 2B by 2C and 2N by 2C models, the N–N bonds in the former model and the C–N bonds of the

latter model support vibration modes that suggest resonant models. The models presented in Fig. 6a and c include boron and nitrogen monovacancies in their sheets, which cause large-scale positive or negative charge distributions around the absent atoms, as depicted in Fig. 7.

To complement our discussions, we have included the structural formula of all of the models, which indicate the positions of single and conjugated $sp^2$ orbitals (see Figs. 5b, d, and f, 6b, d, f, h, j, l, and n, and 7b, d, and f).

## Conclusions

In this work, we have presented the results of defect engineering studies of boron nitride sheets. We modeled the systems as clusters of coronene isomers, consisting of a hexagon surrounded by three pentagons and three heptagons. Our molecular quantum mechanics studies showed the possible structures formed (with an armchair edge). We also demonstrated how the electronic (HOMO–LUMO gap) and atomic structures of BN sheets can be modified. Changing the polarity modifies mechanical properties such as the chemical hardness. The electric conductivity is modified by the presence of impurities at different concentrations (i.e., by replacing the boron or nitrogen atoms of the central hexagon in the structure with one, two, three, or six carbon atoms) as well as the presence of mono- and divacancies (boron–nitrogen) in the lattice. Studying the electrostatic potential surfaces of the different BN sheet models highlighted changes in the charge distribution caused by doping or lattice defects. Inspecting the isosurfaces elucidated $sp^2$ hybridization-based bond formation.

**Acknowledgments** This work was partially supported by VIEP-Benemérita Universidad Autónoma de Puebla (CHAE-ING1I-I), Facultad de Ingeniería Química-Benemérita Universidad Autónoma de Puebla (2010–2011), Cuerpo Académico Ingeniería en Materiales (BUAP-CA-177), Cuerpo Académico Física Computacional de la Materia Condensada (BUAP-CA-191), and VIEP-BUAP--EXC. Work performed by GHC was supported by Conacyt project # 83982. GHC's work was also partly performed while visiting the Department of Physical and Theoretical Chemistry, University of Saarland, Saarbruecken, Germany.

## References

1. Novoselov KS, Jiang D, Schedin F, Booth TJ, Khotkevich VV, Morozov SV, Geim AK (2005) Proc Natl Acad Sci USA 102:10451–10453
2. Serrano J, Bosak A, Arenal R, Krisch M, Watanabe K, Taniguchi T, Kanda H, Rubio A, Wirtz L (2007) Phys Rev Lett 98:095503–095504
3. Appelhans DJ, Lin Z, Lusk MT (2010) Phys Rev B 82:073410–073414
4. Akcöltekin S, Bukowska H, Peters T, Osmani O, Monnet I, Alzaher I, d'Etat BB, Lebius H, Schleberger M (2011) Appl Phys Lett 98:103103–3
5. Lahiri J, Lin Y, Bozkurt P, Oleynik II, Batzill M (2010) Nature Nanotech 5:326–329
6. Ciesielski A, Cyranski MK, Krygowski TM, Fowler PW, Lillington M (2006) J Org Chem 71:6840–6845
7. Zeng H, Zhi C, Zhang Z, Wei X, Wang X, Guo W, Bando Y, Golberg D (2010) Nano Lett 10:5049–5055
8. Chigo Anota E (2009) Superficies y Vacío 22:19–23
9. Chigo Anota E, Hernández Cocoletzi H (2011) J Mol Model. doi:10.1007/s00894-011-1043-2
10. Chigo Anota E, Salazar Villanueva M, Hernández Cocoletzi H (2010) Phys Stat Solidi C 7:2252–2254
11. Chigo Anota E, Salazar Villanueva M (2009) Superficies y Vacío 22:23–28
12. Chigo Anota E, Salazar Villanueva M, Hernández Cocoletzi H (2010) Phys Stat Solidi C 7:2559–2561
13. Chigo Anota E, Hernández Cocoletzi H, Rubio Rosas E (2011) Eur Phys J D 63:271–273
14. Chigo Anota E, Hernández Cocoletzi H, Bautista Hernández A, Sánchez Ramírez JF (2011) J Comput Theor Nanosci 8:637–641
15. Kohn W, Becke AD, Parr RG (1996) J Phys Chem 10:12974–12980
16. Jones RO, Gunnarsson O (1989) Rev Mod Phys 61:689
17. Kohn W (1999) Rev Mod Phys 71:1253–1266
18. Parr R, Yang W (1989) Density functional theory of atoms and molecules, 1st edn. Oxford University Press, New York
19. Chigo Anota E, Rivas Silva JF (2005) Rev Col Fís 37:405–417
20. Delley B (1990) J Chem Phys 92:508–608
21. Perdew JP, Wang Y (1992) Phys Rev B 45:13244–13249
22. Delley B (1996) J Phys Chem 100:6107–6110
23. Delley B (2000) J Chem Phys 113:7756–7765
24. Foresman JB, Frisch Æ (1996) Exploring chemistry with electronic structure methods, 2nd edn. Gaussian, Inc., Pittsburgh, p 70
25. Hernández Rosas JJ, Ramírez Gutiérrez RE, Escobedo Morales A, Chigo Anota E (2010) J Mol Model 17:1133–1139
26. Galicia Hernández JM, Hernández Cocoletzi G, Chigo Anota E (2011) J Mol Model. doi:10.1007/s00894-011-1046-z
27. Weiner PK, Langridge R, Blaney JM, Schaefer R, Kollman P (1982) Proc Natl Acad Sci USA 79:3754–3758
28. Politzer P, Laurence PR, Jayasuriya K (1985) Environ Health Perspect 61:191–202
29. Becke AD (1993) J Chem Phys 98:5648–5652
30. Petersson GA, Al-Laham MA (1994) J Chem Phys 94:6081–6091
31. Petersson GA, Bennett A, Tensfeldt TG, Al-Laham MA, Shirley WA, Mantzaris J (1988) J Chem Phys 89:2193–2219
32. Frisch MJ et al (2004) Gaussian 03, revision C.02. Gaussian, Inc., Wallingford
33. CSC—IT Center for Science Ltd. (2011) g0penMol software download webpage.http://www.csc.fi/english/pages/g0penMol. Last accessed Jan 2011
34. Chigo Anota E, Hernández Cocoletzi H (2011) J Mol Model. doi:10.1007/s00894-011-1043-2
35. Alem N, Erni R, Kisielowski C, Rossell MD, Gannett W, Zettl A (2009) Phys Rev B 80:155425–155432
36. Chigo Anota E, Salazar Villanueva M, Hernández Cocoletzi H (2011) J Nanosci Nanotechnol 11:5515–5518
37. Peralta-Inga Z, Murray JS, Edward Grice M, Boyd S, O'Connor CJ, Politzer P (2001) J Mol Struc THEOCHEM 549:147–158
38. Scrocco E, Tomasi J (1973) Top Curr Chem 42:95–170
39. Naray-Szabo G, Ferenczy GG (1995) Chem Rev 95:829–847
40. Politzer P, Murray JS, Lane P, Concha MC, Jin P, Peralta-Inga Z (2005) J Mol Model 11:258–264
41. Peralta-Inga Z, Lane P, Murray JS, Boyd S, Grice ME, O'Connor CL, Politzer P (2003) Nano Lett 3:21–28